Hindawi Publishing Corporation
Mathematical Problems in Engineering
Volume 2013, Article ID 216982, 11 pages
http://dx.doi.org/10.1155/2013/216982

Research Article

Slide Mode Control for Integrated Electric Parking Brake System

Bin Wang,[1] Xuexun Guo,[1] Chengcai Zhang,[1] Zhe Xiong,[1] Huan Xia,[1] and Jie Zhang[2]

[1] *Hubei Key Laboratory of Advanced Technology of Automotive Parts, Wuhan University of Technology, Wuhan 430070, China*
[2] *Wanxiang Group Technology Center, Hangzhou 310000, China*

Correspondence should be addressed to Xuexun Guo; guoxx@whut.edu.cn

Received 25 October 2013; Accepted 27 October 2013

Academic Editor: Hui Zhang

The emerging integrated electric parking brake (IEPB) system is introduced and studied. Through analyzing the various working stages, the stages switched IEPB system models are given with the consideration of the friction and system idle inertia. The sliding mode control (SMC) method is adopted to control the clamping force by the widely used motor angle and clamping force relationship method. Based on the characteristics of the state equations, two sliding surfaces are built to control the motor angle and current, respectively. And in every working stage, the control stability is guaranteed by choosing the control parameters based on Lyapunov theory and SMC reachability. The effectiveness of the proposed control system has been validated in Matlab/Simulink.

1. Introduction

Lots of strong points exist in X-by-wire systems, such as component number reduction, weight reduction, and performance improvement [1, 2]. Electronic parking brake (EPB) system is one kind of brake-by-wire systems, which generates the parking force by motor torque instead of the manual force. Hence, the EPB system can increase the vehicle cabin space, facilitate the parking process, and have potential function [3]. There are mainly two kinds of EPB: the first one generates the force by pulling down traditional parking cable, as seen in [3–9]. The second one is called integrated EPB (IEPB), which has the similar structure with the electromechanical brake [10–12] and hence it can offer numerous possibilities [13]. IEPB actuator is mounted on the traditional caliper. Through screw-nut structure, the rotating movement from the DC motor can be transformed to the rectilinear motion of the nut [14]. By the moving forward or backward of the nut, the braking force can be generated or released. Once the desired braking force is reached, the motor power can be cut off and the clamping force can be steady due to the screw-nut self-locking.

While IEPB system has been used in some advanced sedans [15, 16], there is very little published research. For EPB with traditional cables, Lee et al. studied the bang-bang [4], nonlinear P controllers [3, 6, 7] to control the clamping force and the controller stability is also analyzed in [3, 7]. The traditional EPB system models were built in [3–7]; however, motor friction and screw-nut system inertia were neglected. Actually, during the motor idle stage, the motor friction and the nut inertia have direct effects on the modeling precision. For IEPB system, due to the limited installation space and the high cost of force sensor, clamping force estimation methods based on the motor position have been proposed in [1, 10–12]. From the researches [10–12, 17], we know based on the angular displacement of the motor that the clamping force can be estimated precisely. However, few control methods that can track the desired motor angle precisely for electric parking brake system are shown in published researches. Especially, robust control, hardly guaranteed by the published control methods, is very important for vehicle safety system [18, 19]. Hence, the authors proposed the sliding mode control method based on the system characteristics to optimize the control precision and robustness [20–22].

The present authors have made much effort over a long time to research and develop EPB system [14, 23, 24]. And to the authors' best knowledge, little published research is about the IEPB system. The main contributions of this paper lie in three aspects. First, this is among the first attempts to develop a detailed system model for IEPB system. In particular, the state-switched system stages and also the motor and screw-nut friction model are considered seriously. Second, this is

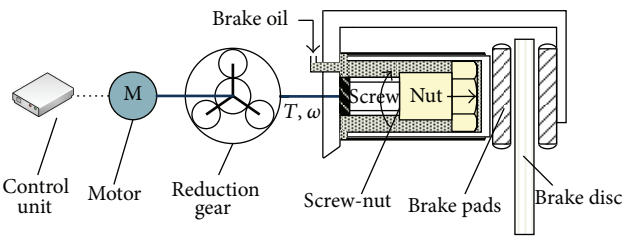

Figure 1: Structure of the IEPB system.

the first attempt to integrate a sliding mode control (SMC) method with EPB system. Through the SMC method, both the precision and robustness of IEPB system are improved apparently. Third, two sliding surfaces are designed to improve the control performance and the control system stability is studied based on Lyapunov theory and system reachability.

The rest of this paper is organized as follows. In the second section, principle and model of the state-dependent IEPB system, including the DC motor and screw-nut system as well as the clamping force, are given. The third section proposed the SMC control law with the proof of the control stability. The simulations and analyses of the proposed control system are shown in the fourth section, followed by the concluding remarks in the final section.

2. System Modeling

In this section, the system structure and system modeling will be presented. The IEPB is a system that locks the vehicle wheels steadily by controlling the motor when receiving the parking brake command. The structure of IEPB system is shown in Figure 1, including DC motor, reduction gears, screw-nut module, traditional brake pads, and disc.

2.1. DC Motor. In IEPB system, the final parking braking force is provided by the motor torque. As shown in Figure 1, motor torque is first transferred to the reduction gears for increasing the driven torque. The model of DC motor can be built as

$$\begin{aligned} U &= L_a \dot{i}_a + R_a i_a + K_{\text{emf}}\omega, \\ K_{\text{motor}} i_a &= J_m \dot{\omega}_m + T_F + T_G, \\ T_m &= K_{\text{motor}} i_a, \end{aligned} \tag{1}$$

where U is the motor voltage; L_a is the inductance; i_a is the motor current; R_a is the resistance; K_{emf} is the EMF constant; ω is the angular rate; T_m is motor torque; K_{motor} is motor constant; T_F is the friction torque, including the viscous friction, dynamical friction T_{FC}, and the maximum static friction $T_{F\max}$; T_G is the load torque; J_m is the moment of inertia of this system. Based on the Armstrong friction model [25], the friction torque of DC motor can be described as

$$T_F = T_{FC} + \left(T_{F\max} - T_{FC}\right) e^{-|\omega/\omega_s|^{\delta_s}} + b_v\omega, \quad (\omega \neq 0), \tag{2}$$

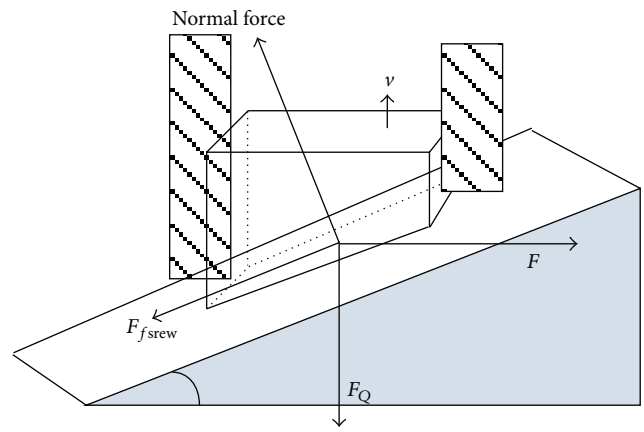

Figure 2: The equivalent structure of screw-nut.

where ω_s is the Stribeck velocity that describes the continuous decrease instead of the break point; δ_s is a coefficient for Stribeck friction.

For simplicity of the analysis, the friction torque can be written as

$$T_F = b_v\omega_m. \tag{3}$$

2.2. Screw-Nut System. In IEPBs, the nut can just move in the axial direction, secured against twisting; on the contrary, the screw can just rotate without moving forward or backward. When the screw rotates in counter-clockwise direction, the head will move forward to the left side in the axial direction. Figure 2 shows the equivalent structure of the screw-nut. The lower wedge denotes the screw while the upper one denotes the nut. Therefore, the relative motion for nut and screw can be seen as the nut is sliding along the slope with an angle inclination α [26–28].

According to the equivalent schematic diagram of screw-nut, the relationship between the screw torque T_L and F can be described as

$$\begin{aligned} N \cdot T_G &= T_L, \\ T_L &= F \cdot r, \end{aligned} \tag{4}$$

where N is the gear ratio between the motor and the IEPB actuator; r is the screw pitch radius; F is the equivalent force on the nut cross section shown in Figure 2. When the nut is moving on the screw, the friction force $F_{f\text{srew}}$ in the screw-nut system can be written as

$$F_{f\text{srew}} = F_{\text{coulomb}\_f} + \left(F_{\max\_f} - F_{\text{coulomb}\_f}\right) e^{-|v/v_s|^2} + c_v v, \tag{5}$$

where $F_{f\text{srew}}$ is the friction force of the screw-nut system; v_s is the Stribeck velocity; c_v is the viscous friction coefficient; $F_{\max\_f}$ is the maximum static friction; F_{coulomb_f} is the coulomb friction proportional to the normal force.

Due to the clearance existing between the nut and the brake disc, the nut needs to move forward first to clear this

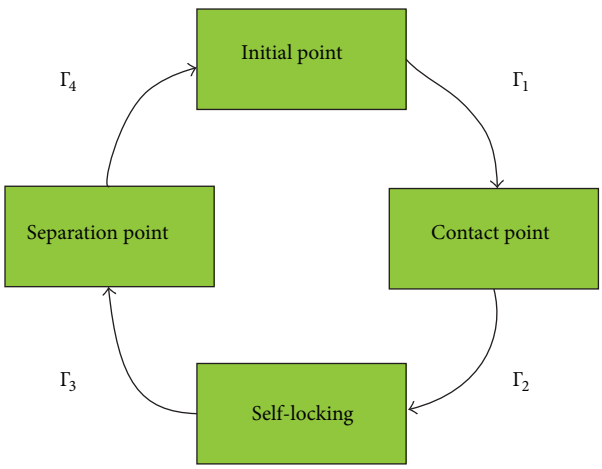

Figure 3: State switched screw-nut system.

gap. This status is named Γ_1 as shown in Figure 3 and it is obvious that there is no clamping force due to no contacting during Γ_1. However, in order to estimate the contact point precisely, the friction torque analysis in screw-nut system is still needed. Stages Γ_1 and Γ_4 have the similar dynamics equations though the speed direction is contrary. While Stages Γ_2 and Γ_3 have the similar dynamics equations, they have a contrary speed direction. Hence, for simplicity of the modeling process, only Γ_1 and Γ_2 are analyzed in this paper.

For Stages Γ_1. Due to no clamping force in Γ_1, the friction force can be written as

$$F \cdot \cos\alpha = F_{f\,\text{srew}}, \tag{6}$$

where α is the lead angle. When there is no contact, the $F_{\text{coulomb\_}f}$ can be ignored and the viscous friction is playing a leading role in (5). Substituting (3) and (4) into (6), it yields

$$\frac{c_v \dot{x}_{\text{nut}}}{\sin\alpha} + \frac{m\ddot{x}_{\text{nut}}}{\sin\alpha} = T_L \cdot \cos\alpha, \tag{7}$$

$$T_L = 2r \cdot \frac{c_v \dot{x}_{\text{nut}} + m_{\text{nut}}\ddot{x}_{\text{nut}}}{\sin 2\alpha}, \tag{8}$$

where m is the mass of the nut. The state equations for the IEPBs in Γ_1 can be presented as

$$\frac{d}{dt}\begin{bmatrix} i \\ \omega \\ \theta \end{bmatrix} = \begin{bmatrix} -\dfrac{R_a}{L_a} i - \dfrac{K_{\text{emf}}}{L_a}\omega + \dfrac{1}{L_a}U \\ \dfrac{K_{\text{motor}} i}{J_m} - \dfrac{b_v \omega}{J_m} - \dfrac{2r\left(c_v \dot{x}_{\text{nut}} + m_{\text{nut}}\ddot{x}_{\text{nut}}\right)}{J_m N \sin 2\alpha} \\ \omega \end{bmatrix}. \tag{9}$$

For Stages Γ_2. During the clamping stage Γ_2, based on the horizontal and perpendicular forces on the contact surface in Figure 2 and due to the much higher magnitude coulomb friction force, the friction force can be written as

$$F_{f\,\text{srew}} = \begin{cases} \dfrac{1}{r} T_L \cos\alpha - F_Q \sin\alpha & v = 0,\ \Delta F < F_{\max\_f} \\ F_{\max\_f}\,\text{sgn}\,(\Delta F) & v = 0,\ \Delta F \geq F_{\max\_f} \\ \mu_s \cdot \dfrac{T_L \sin\alpha + F_Q \cos\alpha r}{r} & v \neq 0, \end{cases} \tag{10}$$

where μ_s is the coulomb friction coefficient; F_Q is the axial load on the nut; ΔF is the external force, deciding the friction direction. Ignoring the little inertia effect of the nut mass during Γ_2 for simplifying modeling, according to Figure 2, the relationship between the screw torque T_L and the head load F_Q can be written as

$$T_L \cdot \frac{1}{r \cdot \tan\left(\alpha + \arctan\mu_s\right)} = F_Q + m_{\text{nut}}\ddot{x}_{\text{nut}}, \tag{11}$$

where m_{nut} is the mass of head and x_{nut} is the linear displacement of head.

According to (8)–(11), the T_L can be written as

$$T_L = \begin{cases} 2r \cdot \dfrac{c_v \dot{x}_{\text{nut}} + m_{\text{nut}}\ddot{x}_{\text{nut}}}{\sin 2\alpha} & \text{during } \Gamma_1 \\ \dfrac{F_Q + m_{\text{nut}}\ddot{x}_{\text{nut}}}{\sigma_1} & \text{during } \Gamma_2, \end{cases} \tag{12}$$

where

$$\sigma_n = \frac{1}{r \cdot \tan\left(\arctan\,\mu + \alpha\right)}. \tag{13}$$

2.3. Clamping Force Model. As shown in Figure 4, A_0, A_c, and A_1 are three points, namely, the nut initial point, nut contact point, and the system contact point, respectively. In clamping maneuver, the nut moves from point A_0 to point A_c and then pushes the pads to clamp the disc and then moves back to initial point A_0 during $\Gamma_{3,4}$. Line d_1 is the gap between the nut initial position A_0 and the piston position. Line d_2 is the total thickness of pad and piston and is a constant value under no pressure. To simplify analyses, the piston and pad are considered as an assembly and we assume no gap exists between the pad and piston. Line d_3 represents the gap between the friction pads to braking disc, which can be guaranteed by the seal groove mechanism. Line d_4 is not shown in Figure 4, since it is the deformation value. With the gap cleared, clamping force will be generated by the nut translational motion.

Nut rectilinear movement x_{nut} can be written as

$$x_{\text{nut}} = d_1 + d_3 + d_4. \tag{14}$$

Based on Newton's laws of motion, the clamping force can be written as

$$F_Q(t) = 2 \cdot \left(k_{\text{brake}} \cdot d_4(t) + b_{\text{brake}} \cdot \dot{d}_4(t)\right), \tag{15}$$

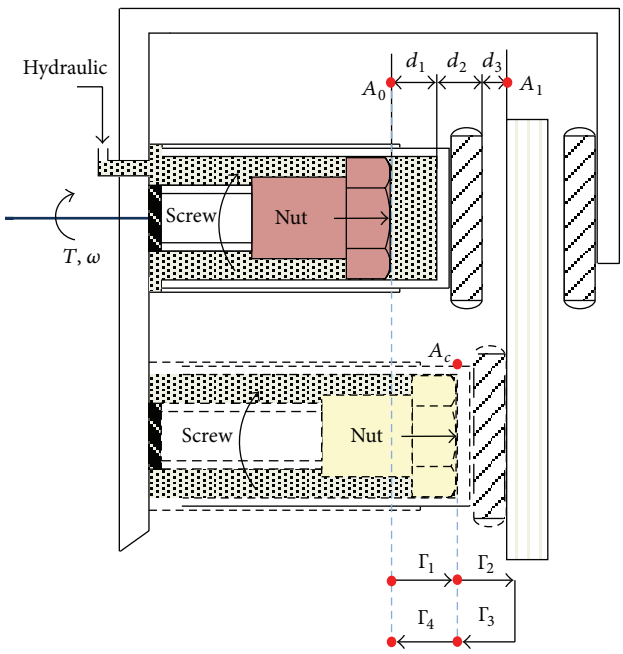

FIGURE 4: Schematic diagram of the IEPBs.

where b_{brake} is the damping coefficient and the overall stiffness of actuator k_{brake} can be calculated from each individual part [1]:

$$k_{\text{brake}} = \frac{1}{1/k_{\text{disk}} + 1/k_{\text{head}} + 2/k_{\text{pad}} + 1/k_{\text{caliper}}}, \tag{16}$$

where k_{brake} is stiffness coefficient of the brake system; k_{disk}, k_{head}, k_{pad}, and k_{caliper} are the stiffness coefficient of brake disc, nut, pad, and the caliper, respectively; θ_L is the angular displacement corresponding to the normal gap distance and is a constant value; θ is the total angular displacement, which can be described as

$$\frac{d_1 + d_3}{\theta_L} = \frac{p}{2\pi N}, \qquad \frac{x_{\text{nut}}}{\theta} = \frac{p}{2\pi N}, \tag{17}$$

$$d_4 = \frac{P}{2\pi N}\tilde{\theta}, \tag{18}$$

where $\tilde{\theta} = \begin{cases} \theta - \theta_L, & \theta > \theta_L \\ 0, & \theta \le \theta_L \end{cases}$ is the active angular displacement corresponding to the compression movement d_4 and p is the pitch of screw:

$$F_Q(t) = 2 \cdot \left(k_{\text{brake}} \cdot \frac{P}{2\pi N}\tilde{\theta} + b_{\text{brake}} \cdot \frac{P}{2\pi N}\dot{\tilde{\theta}} \right). \tag{19}$$

Based on (1) and (12)–(19), the state equations for the IEPBs in Γ_2 can be presented as

$$\frac{d}{dt}\begin{bmatrix} i \\ \omega \\ \theta \end{bmatrix} = \begin{bmatrix} -\dfrac{R_a}{L_a} i - \dfrac{K_{\text{emf}}}{L_a}\omega + \dfrac{1}{L_a}U \\ \dfrac{K_{\text{motor}} i}{J_m} - \dfrac{b_v \omega}{J_m} - \dfrac{p k_{\text{brake}}\tilde{\theta} + p b_{\text{brake}}\omega + m_{\text{head}} p \ddot{\theta}}{2 J_m \pi \sigma_1 N^2} \\ \omega \end{bmatrix}. \tag{20}$$

3. Control Design

Based on (15) and researches in [1, 3–7, 12], we know that the clamping force has a direct relationship with the motor angle. In this paper, a robust control system is designed to track the desired motor angle precisely and then to reach the desired force. Rearranging (9) into standard state space for stage Γ_1 yields

$$\frac{d}{dt}\begin{bmatrix} i \\ \omega \\ \theta \end{bmatrix} = A_{\Gamma_1}\begin{bmatrix} i \\ \omega \\ \theta \end{bmatrix} + B_{\Gamma_1} U, \tag{21}$$

where

$$A_{\Gamma_1} = \begin{bmatrix} -\dfrac{R_a}{L_a} & -\dfrac{K_{\text{emf}}}{L_a} & 0 \\ K_{\text{motor}}\xi & -(b_v + \psi)\xi & 0 \\ 0 & 1 & 0 \end{bmatrix}, \tag{22}$$

$$B_{\Gamma_1} = \begin{bmatrix} \dfrac{1}{L_a} \\ 0 \\ 0 \end{bmatrix}, \tag{23}$$

$$\psi = \frac{\text{rcp}}{\pi N^2 \sin 2\alpha}, \tag{24}$$

$$\xi = \frac{\pi N^2 \sin 2\alpha}{J_m \pi N^2 \sin 2\alpha + \text{rpm}_{\text{nut}}}. \tag{25}$$

Rearranging (20) into standard state space for state Γ_2 yields

$$\frac{d}{dt}\begin{bmatrix} i \\ \omega \\ \theta \end{bmatrix} = A_{\Gamma_2}\begin{bmatrix} i \\ \omega \\ \theta \end{bmatrix} + B_{\Gamma_2} U, \tag{26}$$

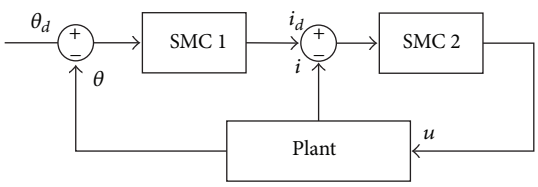

Figure 5: Schematic diagram of the SMC system.

where

$$A_{\Gamma_2} = \begin{bmatrix} -\dfrac{R_a}{L_a} & -\dfrac{K_{\text{emf}}}{L_a} & 0 \\ K_{\text{motor}}\varphi_n & -(b_v + \kappa_n)\varphi_n & -\delta_n\varphi_n \\ 0 & 1 & 0 \end{bmatrix}, \quad B_{\Gamma_2} = \begin{bmatrix} \dfrac{1}{L_a} \\ 0 \\ 0 \end{bmatrix}, \tag{27}$$

where

$$\kappa_n = \frac{p \cdot b_{\text{brake}}}{2\pi\sigma_n N^2}, \quad \delta_n = \frac{p \cdot k_{\text{brake}}}{2\pi\sigma_n N^2}, \quad \varphi_n = \frac{2\pi\sigma_n N^2}{2\pi\sigma_n J_m N^2 + m_{\text{head}} p}. \tag{28}$$

For all the dynamic stages Γ_{1-4}, the feedback can be chosen as

$$y = \begin{bmatrix} 0 & 0 & 1 \end{bmatrix} \begin{bmatrix} i \\ \omega \\ \theta \end{bmatrix}. \tag{29}$$

3.1. Control Law Design. The control robustness is very important [29], especially for braking system. In this part, a sliding mode control (SMC) design procedure for the state-switched IEPB system is presented, which mainly includes 2 steps: firstly, the design of the sliding surface; secondly, the design of the controller, by which the trajectory will be guided to sliding on the surface designed in step one. Note that the clamping force has a direct relationship with the angular displacement $\tilde{\theta}$ based on (18) and (19). From (21), (26), and (29), we know the control input u can just directly control the current; however, current i has a relationship with the angular displacement. Hence, we define two sliding surfaces as shown in Figure 5 for angular displacement control and current control, respectively.

These two sliding surfaces are defined as

$$s_1 = \dot{e}_1 + g e_1, \quad (g > 0), \qquad s_2 = i_d - i, \tag{30}$$

where s_1 and s_2 are two sliding surfaces for angular displacement and motor current and $e_1 = \theta_d^* - \theta$, g is a positive gain.

The corresponding control inputs can be written as

$$i_d = \begin{cases} H_{1,\Gamma_1}\,\text{sgn}(s_1) + \dfrac{s_1}{H_{1,\Gamma_1}}, & \text{during } \Gamma_1 \\ H_{1,\Gamma_2}\,\text{sgn}(s_1) + \dfrac{s_1}{H_{1,\Gamma_2}}, & \text{during } \Gamma_2, \end{cases} \tag{31}$$

$$u = \begin{cases} H_{2,\Gamma_1}\,\text{sgn}(s_2) + \dfrac{s_2}{H_{2,\Gamma_1}}, & \text{during } \Gamma_1 \\ H_{2,\Gamma_2}\,\text{sgn}(s_2) + \dfrac{s_1}{H_{2,\Gamma_2}}, & \text{during } \Gamma_2, \end{cases} \tag{32}$$

where $H_{i,\Gamma_j(i,j=1,2)}$ are the control parameters which need to be determined.

Remark 1. The current i_d is a virtual input to connect the desired angular displacement and the actual control input u.

Remark 2. If $H_{i,\Gamma_j(i,j=1,2)}$ is a very small value and $1/H_{i,\Gamma_j(i,j=1,2)}$ will be a large value, which can help reduce the chattering when the state trajectories are closing to the sliding surfaces and can also apply a higher gain for larger error.

Remark 3. $H_{i,\Gamma_j(i,j=1,2)}$ should be chosen to make the sliding surface satisfy the reachability condition as follows [20]:

$$\frac{1}{2}\frac{d}{dt}\left(s(t)^2\right) \le -\eta\,|s(t)|, \quad \eta > 0. \tag{33}$$

Theorem 4. *The SMC controller given in* (31) *is asymptotically stable if the gains are chosen as*

$$H_{1,\Gamma_1} > \frac{\eta_1 + |(b_v\xi + \psi\xi - g)\,\omega|}{K_{motor}\xi}, \qquad H_{1,\Gamma_2} > \frac{\eta + |(b_v + \kappa_n - g)\,\omega| + \delta_n\varphi_n\theta}{K_{motor}\varphi_n}. \tag{34}$$

Proof. Select a Lyapunov function candidate for s_1 as

$$V_1 = \frac{1}{2}{s_1}^2, \tag{35}$$

for stage Γ_1.

Substituting (21) and (22) into the first order derivative of (35) yields

$$\dot{V}_1 = \ddot{e}_1 + g\dot{e}_1 = -\left(\frac{d\omega}{dt} + g\omega\right) = (b_v\xi + \psi\xi - g)\,\omega - K_{\text{motor}} i\xi. \tag{36}$$

Based on Remark 3, we have

$$\frac{1}{2}\frac{d}{dt}\left(s_1(t)^2\right) \le -\eta_1\,|s_1(t)|, \quad \eta_1 > 0, \tag{37}$$

when $s_1 > 0$; substituting (31) and (36) into (37),we have

$$s_1\left[(b_v\xi + \psi\xi - g)\,\omega - K_{\text{motor}} i\xi\right] \le -\eta_1 s_1, \tag{38}$$

$$H_{1,s_1>0,\Gamma_1} > \frac{\eta_1 + (b_v\xi + \psi\xi - g)\,\omega}{K_{\text{motor}}\xi}, \tag{39}$$

when $s_1 < 0$; we have

$$s_1\left[\left(b_v\xi + \psi\xi - g\right)\omega - K_{\text{motor}}i\xi\right] \le -\eta_1 s_1, \tag{40}$$

$$H_{1,s_1<0,\Gamma_1} > \frac{\eta_1 - \left(b_v\xi + \psi\xi - g\right)\omega}{K_{\text{motor}}\xi}. \tag{41}$$

Hence, based on (39) and (41), the reachability can be satisfied if

$$H_{1,\Gamma_1} > \frac{\eta_1 + \left|\left(b_v\xi + \psi\xi - g\right)\omega\right|}{K_{\text{motor}}\xi}, \tag{42}$$

for stage Γ_2.

Substituting (27) into the first time derivative of (35), we have

$$\begin{aligned}\dot{V}_1 &= \ddot{e}_1 + g\dot{e}_1 = -\left(\frac{d\omega}{dt} + g\omega\right)\\ &= \left(b_v + \kappa_n - g\right)\omega + \delta_n\varphi_n\theta - K_{\text{motor}}\varphi_n i.\end{aligned} \tag{43}$$

According to Remark 3, the reachability needs to be satisfied,

$$\frac{1}{2}\frac{d}{dt}\left(s_1(t)^2\right) \le -\eta_1\left|s_1(t)\right|, \quad \eta_1 > 0, \tag{44}$$

when $s_1 > 0$; substituting (31) and (43) into (44),we have

$$\left(b_v + \kappa_n - g\right)\omega + \delta_n\varphi_n\theta - K_{\text{motor}}\varphi_n H_{1,\Gamma_2} < -\eta_1, \tag{45}$$

$$H_{1,s_1>0,\Gamma_2} > \frac{\eta_1 + \left(b_v + \kappa_n - g\right)\omega + \delta_n\varphi_n\theta}{K_{\text{motor}}\varphi_n}, \tag{46}$$

when $s_1 < 0$,

$$\left(b_v + \kappa_n - g\right)\omega + \delta_n\varphi_n\theta + K_{\text{motor}}\varphi_n H_{1,\Gamma_2} > \eta_1, \tag{47}$$

$$H_{1,s_1<0,\Gamma_2} > \frac{\eta_1 - \left(b_v + \kappa_n - g\right)\omega - \delta_n\varphi_n\theta}{K_{\text{motor}}\varphi_n}. \tag{48}$$

Hence, based on (46) and (48), the reachability can be satisfied if

$$H_{1,\Gamma_2} > \frac{\eta_1 + \left|\left(b_v + \kappa_n - g\right)\omega\right| + \delta_n\varphi_n\theta}{K_{\text{motor}}\varphi_n}. \tag{49}$$

□

Theorem 5. *The SMC controller given in* (32) *is asymptotically stable if the gains are chosen as*

$$H_2 \ge \eta L_a + R_a i_a + K_{\text{emf}}\omega, \tag{50}$$

which is the reaching condition for the sliding mode.

Note that due to the fact that Theorem 5 shares the same Lyapunov function with Theorem 4, the proof will not be presented here.

Table 1: IEPBs simulation parameters.

Motor (25–30°C)	R_a	0.465 Ω
	K_{emf}	9.947 mV/rad/sec
	K_{motor}	9.947 m-Nm/Amp
Reduction gear	Gear ratio	150 : 1
Screw-nut	Pitch	2 mm
	radius	5 mm

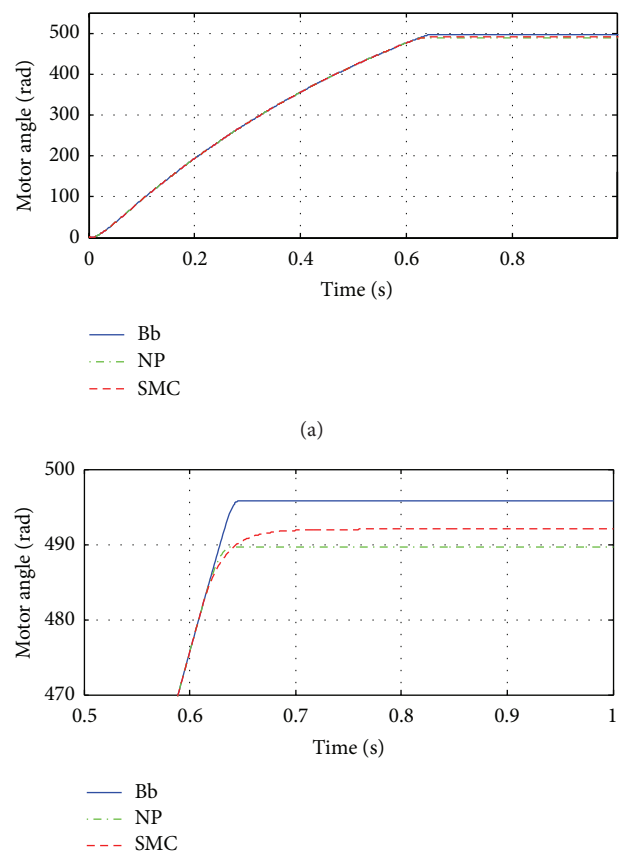

Figure 6: Comparison among three control laws ($\theta_d = 492$ rad). Bb: Bang-bang control. NP: nonlinear Proportion control. SMC: sliding mode control.

4. Simulations and Discussions

In this section, we will study the control performance of the proposed sliding mode control strategy by means of simulation examples. The system parameters and actuator parameters are given in Table 1. The proposed SMC control law is validated by simulation performed in Matlab/Simulink.

Figure 6 shows the target motor angle tracking performance between the Bang-bang control [4], nonlinear Proportion control [3, 7], and sliding mode control with the desired motor angle 492 rad. From Figure 6(a), it is obvious that before 0.6 sec, there is nearly no difference among these three controllers. From Figure 6(b), we can see that the Bang-bang controller leads to a steady state error of 5 rad though it

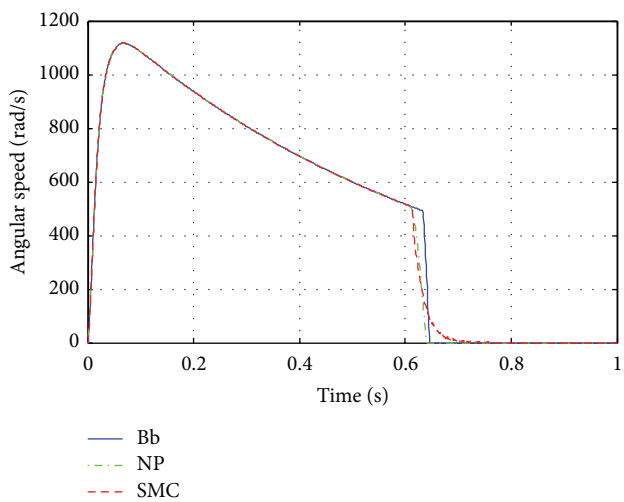

FIGURE 7: Motor speed comparisons among three control laws (θ_d = 492 rad).

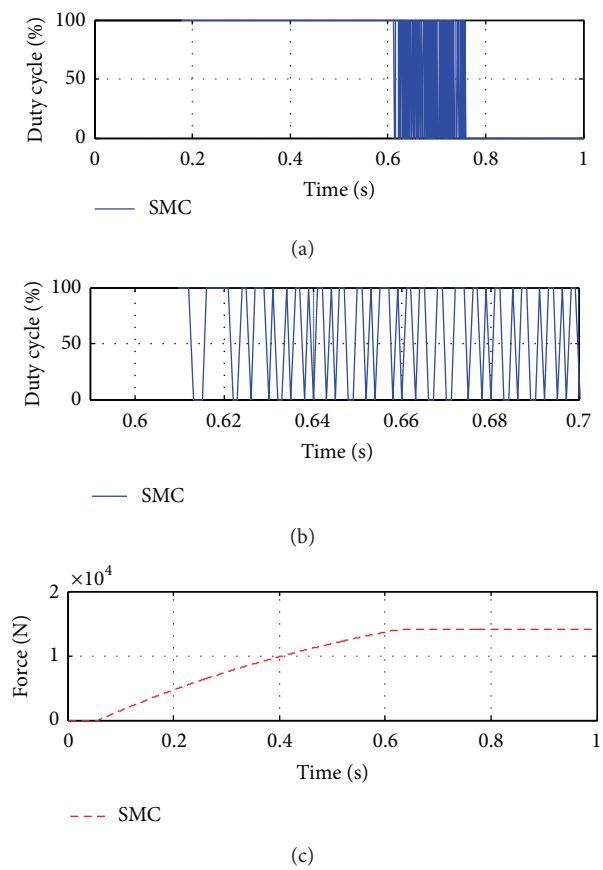

FIGURE 8: Duty cycle and clamping force under SMC (θ_d = 492 rad).

increases to the target first. The nonlinear P controller results in a negative error of 2 rad. In SMC, it is easy to notice that when the motor angle is closing to the target, the gradient is decreasing gradually due to the effects of sliding surfaces. And the SMC controller reaches the 492 rad precisely. Note that for common parking brake maybe the larger force may not lead to dangerous situations. However, IEPBs should have the ability to track the target precisely, because 1 rad angle error can cause hundreds of Newton force error, which may lead to serious condition during the dynamic braking maneuver. On the other hand, compared with the desired clamping force, a larger one can also lead to a releasing problem, since during the releasing mode, the motor needs to rotate contrarily. With the larger clamping force, it may result in a much higher motor current to rotate this nut.

Figure 7 shows the comparisons of three controllers. We can see that before 0.6 s these three speed curves are similar, while after 0.6 s the gradient of SMC speed curve changes due to the sliding surface effect. The NP speed curve gradient also changes based on the angle tracking error. For the bang-bang controller, only if the target 492 rad is reached, the control input will be changed. Hence, based on the analysis of Figure 7, it is easier to understand the motor angle curves in Figure 6.

Based on the analysis for Figures 6 and 7, we know the sliding mode control overmatches the other two control methods with respect to the tracking precision. From Figure 8, we will analyze the control input and the clamping force. In Figure 8(a), the duty cycle of control input is always 100 percent due to the large error before 0.6 s. While from the period 0.6 to 0.77 s shown also in Figure 8(b), it is obvious that the duty cycle is changing fast between 0 and 100 percent, since the trajectory is entering to the sliding surfaces. The clamping force is shown in Figure 8(c). And it can be seen, before 0.06 s, that the clamping force is zero while during the same period the motor angle is increasing to 47 rad as shown in Figures 8(c) and 6. That is because there is gap distance between the nut and the disc that need be cleared first to generate the clamping force.

In order to testify the control robustness with respect to the setpoint value, the desired motor angle is chosen as 300 rad. As can be seen in Figure 9(a), all of these three curves can increase to the value around the target 300 rad and hold steady. From Figure 9(b), it is obvious that the SMC curve reaches the target exactly, while the nonlinear P and Bang-bang have 6.2 rad and 13.6 rad error, respectively.

From Figure 10, we can see that after 0.35 s, the SMC speed curve converges to zero much more gently due to the sliding mode effect when compared with the other two curves. For nonlinear P controller, we can see that due to the nonlinear P control effect, the NP speed curve can change based on the angle error nonlinearly to improve the tracking performance compared with the bang-bang as seen in Figures 9 and 10.

From Figures 11(a) and 11(b), we can see the control input change. The duty cycle is constant 100 percent until 0.31 s. When entering into the sliding surface, the duty cycle of the voltage changes fast to make the trajectory converge to zero. Note that in Figure 11(b), during the period 0.31 s–0.34 s, the duty cycle is also zero. That is because in the first sliding surface $s_1 = \dot{e}_1 + ge_1$, the absolute value of angular speed is larger than the angle error, which results in the negative value of the sliding surface. Correspondingly, the duty cycle

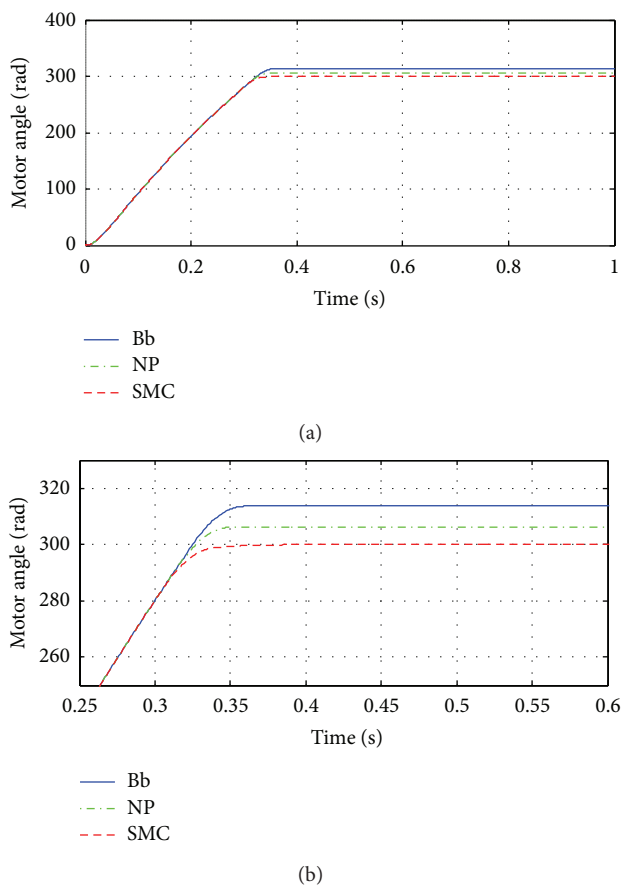

Figure 9: Comparison among three control laws ($\theta_d = 300$ rad).

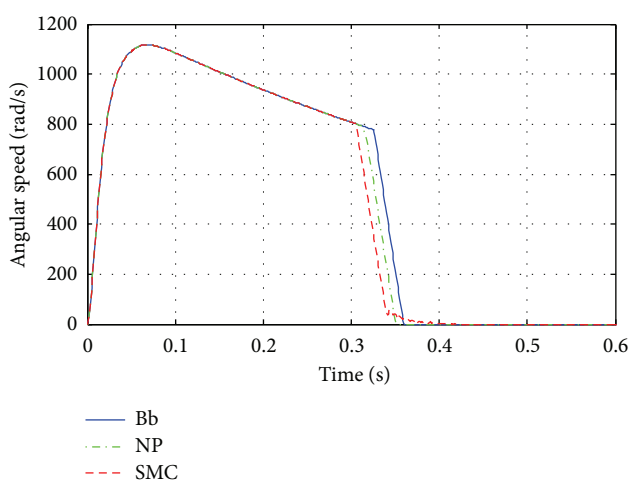

Figure 10: Motor speed comparisons among three control laws ($\theta_d = 300$ rad).

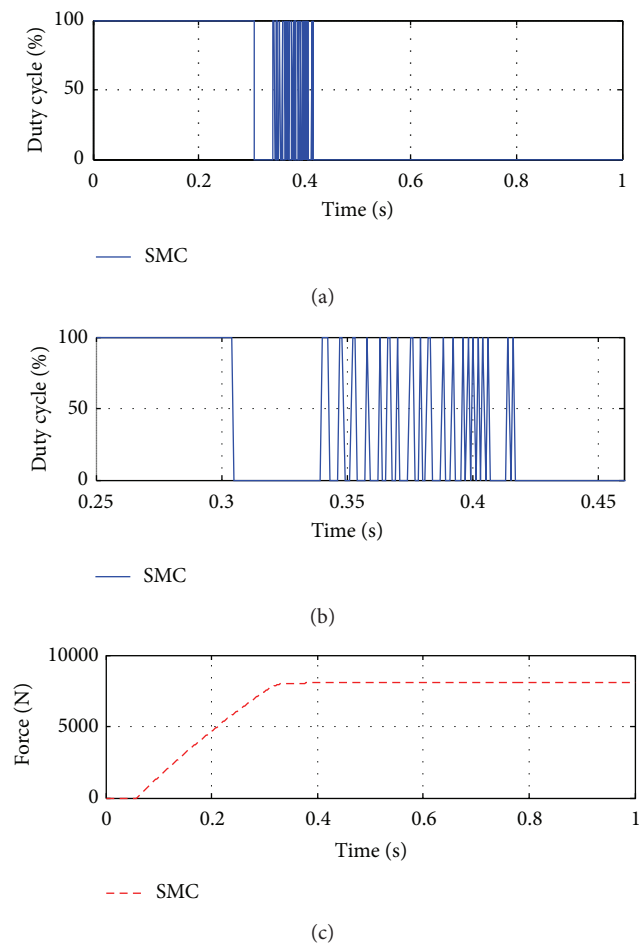

Figure 11: Duty cycle and clamping force under SMC ($\theta_d = 300$ rad).

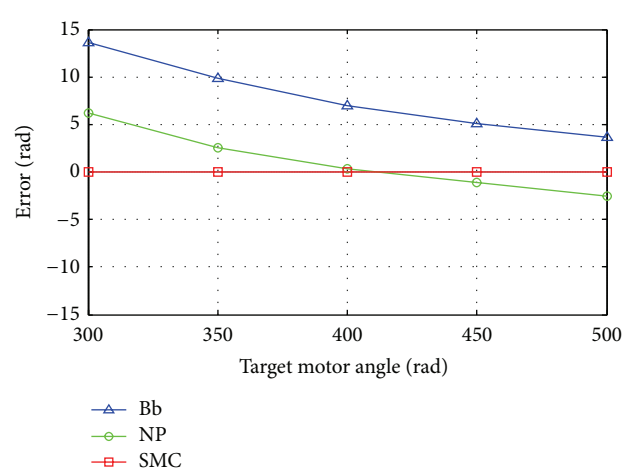

Figure 12: The motor angle errors with three controllers under various set-points.

will be the lowest value to attract the trajectory to zero from the negative orthant. Once the sliding surfaces $s_1 = 0$, $s_2 = 0$ are reached steadily, the motor power can be cut off. The corresponding clamping force is shown in Figure 11(c).

As can be seen in Figure 12, the values of the motor angle errors with three different controllers at each set-point are shown. The positive error implies the redundancy force while the negative erros means the insufficient displacement. Apparently, the SMC curve shows the best performance with no error during the whole targets. NP curve shows the best

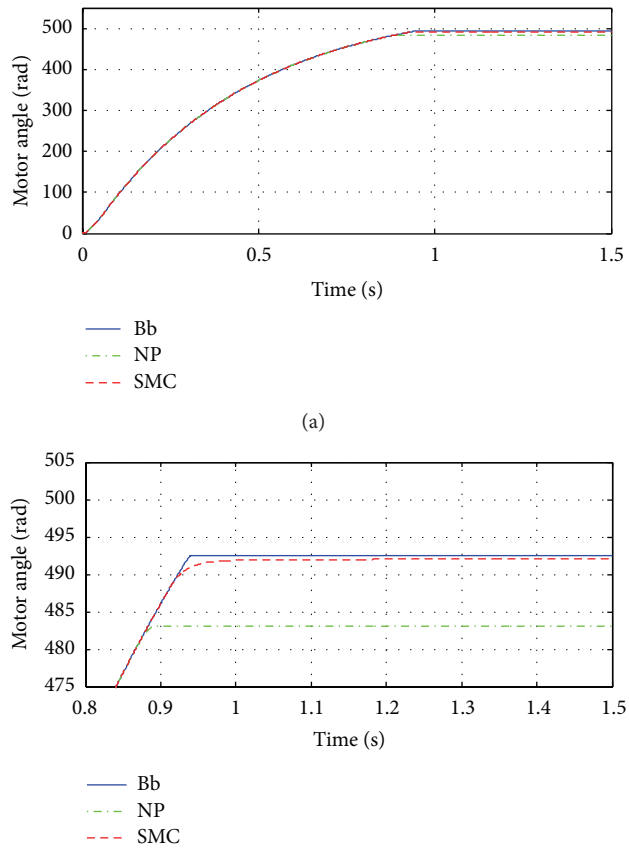

FIGURE 13: The motor angle errors with an increase in screw-nut friction coefficient (θ_d = 492 rad).

performance when the target is 400 rad, while on the other targets the absolute value of the error is increasing. The Bang-bang controller shows the worst performance in terms of the precision, while the error is converging to zero with the increase of the target angle. This good trend may result from the lower angular speed at the power cut-off point.

It is possible that due to the wear of the actuator or the external effects, the friction coefficient of screw-nut system changes. We still take the desired value 492 rad as an example to testify the robustness of these three controllers. The coefficient μ is assumed to change from 0.25 to 0.4 and the performance is shown in Figure 13. Apparently, the NP curve has a larger error, nearly 9 rad, compared with the desired value. Bang-bang shows a better performance with 0.5 rad error, since with the increase of the friction coefficient the angular speed will be lower than the normal status at cut-off point. The SMC curve shows a very good robustness with respect to the friction ratio change.

5. Conclusions

In this paper, a sliding mode control method is utilized to control the clamping force on an integrated electric parking brake system. The working stages are analyzed with a graphical description. By means of the working stages analyses, the stage-switched state-space equations are given with the consideration of friction and system inertia. Based on the system structure from the stage-switched state-space, two sliding surfaces are developed to control the current and angular displacement, respectively. A common Lyapunov function is constructed to guarantee the control system stability. And through the reachability of SMC system, the control gain is also given in this paper. Through these two sliding surfaces, the angle degree set-point can be reached robustly with the gains the scope of which is obtained in the stability section. In the simulation section, three control methods are compared. For each set-point, the Bang-bang controller can track the target but always with a positive error which decreases with the rising of the target displacement; the nonlinear Proportional controller widely used in some published papers can track the target with less error than Bang-bang controller; however, it shows a poor robustness with respect to the friction and set-point variation; the proposed SMC method can track the desired value precisely and robustly. For various set-points, the SMC can track the target value by changing the control input quickly, and under the gain boundary it shows a good robustness with respect to the friction and set-point variation. Based on the relationship between the motor angle and clamping force, the future work is studying the dynamic braking control by IEPBs actuators.

Appendix

Nonlinear P Control

A nonlinear clamping force control law using nonlinear P control theory for traditional EPB system was developed by Lee et al. [3–7]. The control input can be written as

$$u = \begin{cases} K_{p\_nl}|e|^{\alpha}, & \forall e > \delta > 0 \\ K_{p\_nl}\delta^{\alpha-1}, & \forall e \le \delta \\ u_{\min}, & \forall e < 0. \end{cases} \tag{A.1}$$

It applies high gain for small error and small gain for large error.

Nomenclature

b_v: Motor viscous friction coefficient
b_{brake}: Damping coefficient of IEPBs
d_1: Gap between the nut and piston
d_2: Total thickness of pad and piston
d_3: Gap between the friction pad and disc
E_b: Back-EMF voltage
F_f: Friction force
F_v: Screw-nut viscous friction coefficient
$F_{\max\_f}$: Maximum friction force
F_Q: Axial load force
i_a: Motor current
J_m: Moment of inertia
k_{brake}: Stiffness coefficient of the brake system
k_{disk}: Stiffness coefficient of brake disc
k_{head}: Stiffness coefficient of nut
k_{pad}: Stiffness coefficient of pad

k_{caliper}: Stiffness coefficient of and the caliper
K_{emf}: EMF constant
K_{motor}: Motor torque constant
L_a: Inductance
m_{nut}: Mass of nut
N: Gear ratio
R_a: Resistance
T_m: Motor torque
T_F: Motor friction torque
T_L: Screw torque
T_{FC}: Motor dynamic friction torque
$T_{F\max}$: Motor maximum static friction torque
u: Control input
U: Motor Voltage
x_{nut}: Linear displacement of nut
α: Screw lead angle
θ_L: Angular position corresponding to gap
θ: Total angular displacement
ω: Motor angular velocity
ω_s: Stribeck angular velocity
μ_s: Sliding friction coefficient.

Acknowledgments

This work is partially supported by the Fundamental Research Funds for the Central Universities (Grant no. 2012-JL-11), China Scholarship Council Funding (Grant no. 201306950040), and the Wanxiang Group.

References

[1] S. Ralf, R. Isermann, J. Böhm et al., "Clamping force estimation for a brake-by-wire actuator," SAE 1999-01-0482, 1999.

[2] E. A. Bretz, "By-wire cars turn the corner," *IEEE Spectrum*, vol. 38, no. 4, pp. 1–7, 2001.

[3] Y. O. Lee, Y. S. Son, and C. C. Chung, "Clamping force control for an electric parking brake system: switched system approach," *IEEE Transactions on Vehicular Technology*, vol. 62, no. 7, pp. 2937–2948, 2013.

[4] Y. O. Lee, M. Jang, W. Lee, C. W. Lee, C. C. Chung, and Y. S. Son, "Novel clamping force control for electric parking brake systems," *Mechatronics*, vol. 21, no. 7, pp. 1156–1162, 2011.

[5] M. Jang, Y. O. Lee, W. Lee, C. W. Lee, C. C. Chung, and Y. Son, "Novel clamping force control for electric parking brake systems," in *Proceedings of the 7th Asian Control Conference (ASCC '09)*, pp. 1588–1593, Hong Kong, China, August 2009.

[6] Y. O. Lee, C. W. Lee, H. B. Chung et al., "A nonlinear proportional controller for electric parking brake system," SAE 2007-01-3657, 2007.

[7] Y. O. Lee, C. W. Lee, C. C. Chung, Y. Son, P. Yoon, and I.-Y. Hwang, "Stability analysis of an Electric Parking Brake (EPB) systems with a nonlinear proportional controller," in *Proceedings of the 17th World Congress, International Federation of Automatic Control, IFAC*, pp. 14247–14253, Coex, South Korea, July 2008.

[8] C. W. Lee, H. B. Chung, Y. O. Lee, C. C. Chung, Y. S. Son, and P. Yoon, "Fault detection method for electric parking brake (EPB) systems with sensorless estimation using current ripples," *International Journal of Automotive Technology*, vol. 11, no. 3, pp. 387–394, 2010.

[9] K. Kondo and T. Watanabe, Parking brake control system US Patent 8296029 B2, 2012.

[10] S. Saric, A. Bab-Hadiashar, and R. Hoseinnezhad, "Clamp-force estimation for a brake-by-wire system: a sensor-fusion approach," *IEEE Transactions on Vehicular Technology*, vol. 57, no. 2, pp. 778–786, 2008.

[11] C. Line, C. Manzie, and M. Good, "Control of an electromechanical brake for automotive brake-by-wire systems with an adapted motion control architecture," SAE 2004-01-2050, 2004.

[12] C. Jo, S. Hwang, and H. Kim, "Clamping-force control for electromechanical brake," *IEEE Transactions on Vehicular Technology*, vol. 59, no. 7, pp. 3205–3212, 2010.

[13] R. Leiter, "Design and control of an electric parking brake," SAE 2002-01-2583, 2002.

[14] W. Bin, G. Xuexun, Z. Chengcai et al., "Simulation and experiment on electrical parking brake system," *Transactions of the Chinese Society for Agricultural Machinery*, vol. 44, no. 8, pp. 45–49, 2013.

[15] TRW, http://www.trw.com/braking_systems/electric_park_brake/epb.

[16] Mercedes Benz 216 Electric parking brake Control Units, http://www.micro-tronik.com/mercedes_benz_216_electric_parking_brake_(efb)_235.html.

[17] S. Saric, A. Bab-Hadiashar, and J. V. D. Walt, "Estimating clamp force for brake-by-wire systems: thermal considerations," *Mechatronics*, vol. 19, no. 6, pp. 886–895, 2009.

[18] H. Zhang, Y. Shi, and J. Wang, "Observer-based tracking controller design for networked predictive control systems with uncertain Markov delays," *International Journal of Control*, vol. 86, no. 10, pp. 1824–1836, 2013.

[19] H. Zhang, Y. Shi, and M. Liu, "H∞ step tracking control for networked discrete-time nonlinear systems with integral and predictive actions," *IEEE Transactions on Industrial Informatics*, vol. 9, no. 1, pp. 337–345, 2013.

[20] P. Kachroo and M. Tomizuka, "Chattering reduction and error convergence in the sliding-mode control of a class of nonlinear systems," *IEEE Transactions on Automatic Control*, vol. 41, no. 7, pp. 1063–1068, 1996.

[21] H. Zhang, J. Wang, and Y. Shi, "Robust H∞ sliding-mode control for Markovian jump systems subject to intermittent observations and partially known transition probabilities," *Systems & Control Letters*, vol. 62, no. 12, pp. 1114–1124, 2013.

[22] H. Zhang, Y. Shi, and A. Saadat Mehr, "Robust static output feedback control and remote PID design for networked motor systems," *IEEE Transactions on Industrial Electronics*, vol. 58, no. 12, pp. 5396–5405, 2011.

[23] J. Zhang, Y. Tong, X. Zi et al., "Electronic parking brake actuator with cable," Chinese Patent 201120276953.2.

[24] Y. Yong, W. Haotian, G. Xuexun et al., "Design of test bench of the electronic parking brake system," *Chinese Automobile Technology*, vol. 11, no. 1, pp. 40–45, 2012.

[25] H. Olsson, K. J. Åström, C. C. D. Wit, M. Gäfvert, and P. Lischinsky, "Friction models and friction compensation," *European Journal of Control*, vol. 4, no. 3, pp. 1–37, 1998.

[26] O. Vahid and F. Golnaraghi, *Friction-Induced Vibration in Lead Screw Drives*, Springer, New York, NY, USA, 2011.

[27] R. C. Juvinall and K. M. Marshek, *Fundamentals of Machine Component Design*, John Wiley & Sons, New York, NY, USA, 1999.

[28] O. Vahid, N. Eslaminasab, and M. F. Golnaraghi, "Friction-induced vibration in lead screw systems: mathematical modeling and experimental studies," *Transactions of the ASME*, vol. 131, no. 2, pp. 1–10, 2009.

[29] H. Zhang, Y. Shi, and A. S. Mehr, "Robust weighted H_∞ filtering for networked systems with intermittent measurements of multiple sensors," *International Journal of Adaptive Control and Signal Processing*, vol. 25, no. 4, pp. 313–330, 2011.